JOURNAL OF GEOPHYSICAL RESEARCH, VOL. 112, C04017, doi:10.1029/2006JC003641, 2007

Thermal conductivity of landfast Antarctic and Arctic sea ice

D. J. Pringle,[1,2,3] H. Eicken,[2] H. J. Trodahl,[1] L. G. E. Backstrom[2]

Received 12 April 2006; revised 7 September 2006; accepted 18 October 2006; published 24 April 2007.

[1] We present final results from a program to measure the thermal conductivity of sea ice with in situ thermistor arrays using an amended analysis of new and previously reported ice temperatures. Results from landfast first-year (FY) ice near Barrow, Alaska, and McMurdo Sound, Antarctica, are consistent with predictions from effective-medium models but 10–15% higher than values from the parameterization currently used in most sea ice models. We observe no previously reported anomalous near-surface reduction, which is now understood to have been an artifact, nor a convective enhancement to the heat flow, although our analysis is limited to temperatures below −5°C at which brine percolation is restricted. Results for landfast multiyear (MY) ice in McMurdo Sound are also consistent with effective-medium predictions, and emphasize the density dependence. We compare these and historical measurements with effective-medium predictions and the representation commonly used in sea ice models, developed originally for MY Arctic ice. We propose an alternative expression derived from effective-medium models, appropriate for both MY and FY ice that is consistent with experimental results, $k = (\rho/\rho_i)(2.11 - 0.011\,\theta + 0.09\,(S/\theta) - (\rho - \rho_i)/1000)$, where ρ_i and ρ are the density of pure ice and sea ice (kg m^{-3}), and θ (°C) and S (ppt) are sea ice temperature and salinity. For the winter and spring conditions studied here, thermal signatures of internal brine motion were observed rarely (22 times in 1957 days), and their maximum contribution to the total heat flow is estimated to be of the order of a few percent.

Citation: Pringle, D. J., H. Eicken, H. J. Trodahl, and L. G. E. Backstrom (2007), Thermal conductivity of landfast Antarctic and Arctic sea ice, *J. Geophys. Res.*, *112*, C04017, doi:10.1029/2006JC003641.

1. Introduction

[2] Sea ice is an important component in the world climate system, and through a variety of feedback mechanisms it acts as both an indicator and agent of climate change [*Lemke et al.*, 1990; *Dieckmann and Hellmer*, 2003]. To improve the accuracy of sea ice models and general circulation models, accurate representations of both mechanical and thermodynamic sea ice properties and physics are required [e.g., *Dieckmann and Hellmer*, 2003]. Our focus in this study is the thermal conductivity which controls the thermodynamic growth rate, equilibrium thickness, and conductive heat flux through the ice. Considerable uncertainty in the thermal conductivity of sea ice has remained, largely owing to the difficulty in performing measurements, few of which have been made with sufficient accuracy to compare with effective-medium predictions [*Ono*, 1967; *Trodahl et al.*, 2001]. Moreover, the conductivity representation used almost universally in both small- and large-scale sea ice modeling remains essentially unvalidated by measurements.

[3] In this paper we present results from a program started in the mid-1990s to measure the thermal conductivity of sea ice using arrays of thermistor strings frozen into landfast ice. In previously published findings from this program, which we have now concluded, three departures from the expected behavior were observed [*McGuinness et al.*, 1998; *Trodahl et al.*, 2000, 2001]: (1) A conductivity reduction of 25–50% was resolved over the top 50 cm of first-year (FY) ice. (2) Below these depths, an overall reduction of 10% was observed compared with effective-medium predictions. Enhanced phonon scattering due to small crystal size, particularly in the upper frazil ice layer, was proposed as a possible explanation. This effect is indeed responsible for a reduction in the conductivity of pure ice at sufficiently low temperatures (T <100 K) that the mean free path of the phonons is comparable to crystal dimensions [*Slack*, 1980]. (3) An apparent increase in the conductivity was reported for T <−9°C, which was associated with a brine convection enhancement of the local heat flow. This convective effect was more readily accepted than the near-surface reduction, and raised the question of how to measure and include any convective contributions in the total heat flow.

[4] We have reexamined these three previous findings by both performing direct conductivity measurements and by

[1]School of Chemical and Physical Sciences, Victoria University of Wellington, Wellington, New Zealand.
[2]Geophysical Institute, University of Alaska, Fairbanks, Alaska, USA.
[3]Arctic Region Supercomputing Center, University of Alaska, Fairbanks, Alaska, USA.

0148-0227/07/2006JC003641$09.00

continuing the thermistor array program while reviewing our conductivity analysis of these measurements. Results from the new direct measurements on surface and subsurface McMurdo Sound landfast FY ice are consistent with effective-medium predictions and clearly show no reduction over the top 50 cm. They are reported elsewhere, where in the context of the absence of a near-surface conductivity reduction, we also discuss limitations in previous array measurement analysis which we now understand to have given rise to the previously reported anomalous near-surface conductivity reduction [*Pringle et al.*, 2006]. In the present article, we present final results from the combined Victoria University of Wellington (VUW) and University of Alaska Fairbanks (UAF) thermistor array program by applying an amended analysis to both new and previously reported measurements.

[5] In most sea ice models, the thermal conductivity is calculated according to the seminal 1-D thermodynamic sea ice model of *Maykut and Untersteiner* [1971] as

$$k = 2.03 + 0.117\,S/\theta \quad \left[\mathrm{Wm^{-1}K^{-1}}\right] \quad . \tag{1}$$

Here, and throughout this paper, S is sea ice bulk salinity (ppt), θ is temperature in degrees Celsius (°C) and conductivities are given in units of W m^{-1} K^{-1}.

[6] Equation (1) derives from that of *Untersteiner* [1961] which predates almost all theoretical and experimental results. It was chosen to provide a simple closed form that captured the main features of the measurements and predictions available at the time and developed for application to MY Arctic ice [*Maykut and Untersteiner*, 1971]. It is still used in most major models, including the Los Alamos Sea Ice Model (CICE), US National Center of Atmospheric Research (NCAR) Community Atmosphere Model (CAM2), Community Climate System Model (CCSM3.0), Canadian Ice Service Community Ice-Ocean Model (CIOM). Some models use only the constant term from this expression [e.g., *Parkinson and Washington*, 1979; *Lemke et al.*, 1990; *Wu et al.*, 1997], including those applied to Antarctic ice with its much higher fraction of FY ice [e.g., *Lemke et al.*, 1990; *Wu et al.*, 1997]. In their study of the sensitivity of a global sea ice model to model thermodynamics and mechanics, *Fichefet and Maqueda* [1997] used just the constant term, 2.03 W m^{-1} K^{-1}, here seen to have been intended for low-salinity MY ice. The coefficients have been varied in some work, e.g., *Wettlaufer* [1991] used $k = 2.10 + 0.13\ S/\theta$. We are unaware of any models that incorporate convective heat transport. In addition to such large-scale models, equation (1) has also been used for ice-ocean heat flux calculations, and smaller-scale process modeling, for example, by *Vancoppenolle et al.* [2005, 2007] in their 'halo-thermodynamic' modeling of the desalination of FY ice.

[7] The conductivity of sea ice at a given temperature, density and salinity can be predicted with effective-medium models by considering the temperature-dependent conductivity and thermal equilibrium volume fractions of the ice, brine and air components and using an idealized inclusion geometry [*Anderson*, 1958; *Schwerdtfeger*, 1963; *Ono*, 1967; *Yen*, 1981]. As the conductivity of brine is approximately four times smaller than that of ice, the dominant feature in these models is the prediction of a conductivity that decreases as the brine volume increases with increasing temperature. Although several different inclusion geometries have been proposed [*Anderson*, 1958; *Schwerdtfeger*, 1963; *Ono*, 1967; *Yen*, 1981], the ultimate accuracy of these models is limited by the uncertainty in the conductivity of pure ice at 0°C. A major disadvantage of this approach is that these models do not provide simple analytical expressions for the conductivity in terms of density, salinity and temperature. We address this here by fitting a simple analytical form to models appropriate to MY and FY microstructure.

[8] The paper is arranged as follows. We describe our array experiments and analysis, including the recently identified problems and subsequent amendments. We then discuss results from landfast FY and MY Antarctic and landfast FY Arctic ice and compare them against effective-medium predictions and the common modeling representation. In these comparisons we also include results from the small number of historical measurements, compiled here for future reference. We discuss a reassessment of the conductivity parameterization and propose a single alternative expression, derived from effective medium models, applicable to both MY and FY ice. We also describe the observation of thermal signatures linked to internal brine convection and estimate the contribution of such events to the total heat flow.

2. Thermal Array Measurements

[9] We have made in situ ice temperature measurements in landfast sea ice in McMurdo Sound, Antarctica in 1996, 1997, 1999, 2000, 2002, 2003, and in the Chukchi Sea near Barrow, Alaska in 2000, 2001, 2002, 2003. The arrays were installed in auger holes, which refroze naturally. The portion of the hole above freeboard was frozen in by infilling with water. The nearby installation of two arrays, of different and/or identical construction, has enabled an assessment of reproducibility and accuracy of our measurements and a comparison of the different array designs. The reference convention for these arrays follows 'CH03,' and 'MC02(2)' indicating, respectively, Chukchi Sea 2003, and McMurdo Sound 2002, array (2).

[10] Figure 1 shows details of the VUW and UAF arrays. VUW arrays comprised a 6.35-mm-diameter, thin-walled (0.3 mm) 304 stainless steel tube, housing a 2-m length of 3-mm-diameter Teflon, along which YSI55031 thermistor beads were positioned. The small remaining volume was filled with sunflower oil which congeals to a viscous gel at ice temperatures [*McGuinness et al.*, 1998; *Trodahl et al.*, 2000]. The figure of merit regarding thermal mismatch between the array and ice it replaces is the thermal conductance per unit length, which for the VUW array is approximately 30% less than the ice it replaces. Weighted by a larger cross-sectional area, the low conductivity of the Teflon and oil ($\sim$0.2 W m^{-1} K^{-1}) here dominate the higher (but still relatively low) conductivity of the thin-walled stainless steel tube ($\sim$15 W m^{-1} K^{-1}). Low-conductivity constantan wiring was used ($\sim$22 W m^{-1} K^{-1}). UAF arrays were constructed from a 20-mm-wide polycarbonate-polyethylene conduit. The thermal conductance per unit length is dominated by the copper wiring, and varies down the array with the number of wires running to the surface. It ranges between one third and three times that of the ice is replaces.

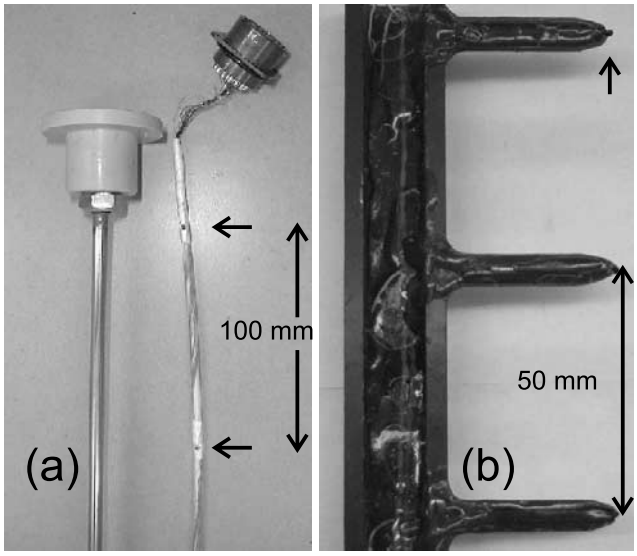

Figure 1. (a) VUW and (b) UAF thermistor strings. Black arrows point to thermistors. The VUW string was slid into a thin-walled stainless steel tube, allowing recycling and servicing. UAF thermistors and wiring were fixed in place with resin. The UAF arrays were painted white prior to deployment in order to minimize solar heating of the arrays.

Thermistors were positioned at the open end of protruding 'fingers' and sealed in place with resin [*Frey et al.*, 2001]. This design optimized the thermal contact between the thermistors and minimally disturbed ice. Prior to deployment, the UAF arrays were painted white. One-point thermistor calibrations were performed from either field measurements of sea water in thermal equilibrium with natural sea ice, or laboratory ice baths. We compare the performance of these different arrays in section 4.2.

[11] Most measurements were made with Campbell Scientific CR10X loggers but some VUW measurements were made with custom-built loggers with an improved temperature precision (see below). In most measurements analyzed here, 10 forward and 10 reverse polarity measurements made in quick succession were averaged for each thermistor for each temperature reading. For the different seasons' measurements, vertical thermistor spacings were $\Delta z = 5$ or 10 cm, and sampling intervals $\Delta t = 10$, 30, or 60 min.

[12] As an example, Figure 2 shows the temperatures measured in FY ice, McMurdo Sound 2002, with a VUW array. Figure 2 (top) shows temperature-time curves for each thermistor. The coldest temperatures correspond to the uppermost thermistor in the ice, $z = 4$ cm. The five lowest thermistors were initially below the ice/water interface, and recorded the water temperature $T_w \approx -1.85$ °C. Figure 2 (bottom) shows the evolution of the temperature depth profile through the season. Not shown are the several days over which thermal (and haline) equilibrium was attained in the refrozen holes. Data from the first week after installation were not analyzed.

3. Conductivity Analysis

[13] We have used a graphical finite difference analysis to extract the conductivity from the measured temperature fields. Following a careful review of our previous such analysis and our equipment, we assessed several factors that

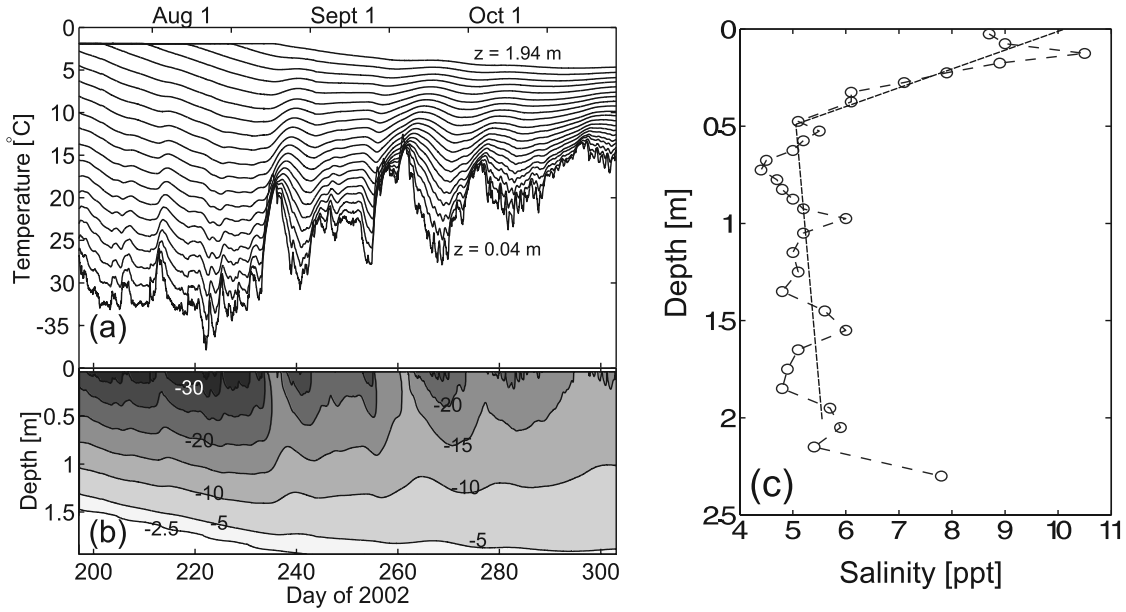

Figure 2. Ice temperatures measured in landfast FY ice, McMurdo Sound, 2002 by VUW array MC02(2). (a) Each line is the temperature-time trace for a given depth. Upper thermistors in the ice recorded the coldest temperatures, and are therefore the lower traces in this figure. When installed, the bottom five thermistors were below the ice/water interface, and recorded the water temperature, $T_w \approx -1.85$°C. (b) Temperature-depth interpolations. (c) Salinity profile from a core extracted when the array was recovered, 11 November 2002. Dashed line is the salinity profile used in our analysis of temperatures measured down to 2 m.

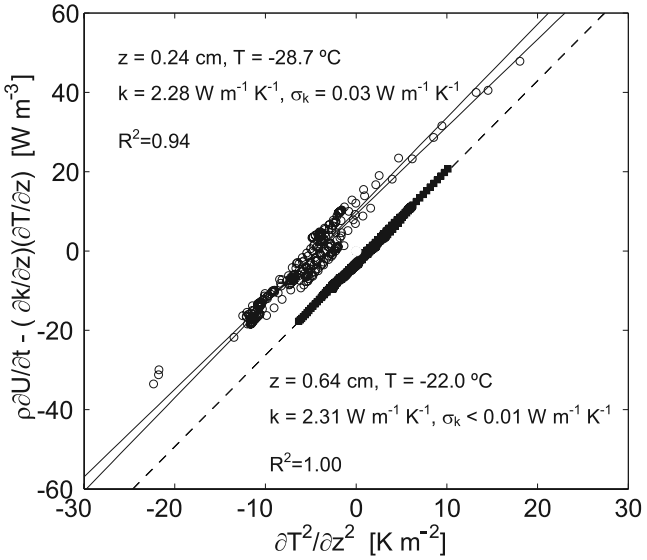

Figure 3. Scatterplots of $\rho\partial U/\partial t - (\partial k/\partial z)(\partial T/\partial z)$ versus $\partial^2 T/\partial z^2$ from measurements in landfast FY McMurdo Sound ice, 3–18 August 2002. Open symbols, 24 cm; solid symbols, 64 cm. Least square fits treating each variable as independent are shown; the two lines for $z = 64$ cm lie on top of each other. Here k is the geometric mean conductivity of the two fitted gradients and σ_k is the standard deviation in this mean.

may have contributed to the three previously reported conductivity anomalies. A full discussion of these aspects is given by *Pringle et al.* [2006]; we now describe the amended analysis applied to obtain the results presented here.

[14] All measurements were made in undeformed, level ice. The small horizontal variations in ice and snow thickness permit a 1-D analysis of the heat flow [*Trodahl et al.*, 2000; *Pringle et al.*, 2006]. Ice temperature variations were related by the following 1-D heat transfer equation,

$$\rho\frac{\partial U}{\partial t} = k\frac{\partial^2 T}{\partial z^2} + \frac{\partial k}{\partial z}\frac{\partial T}{\partial z} \quad , \tag{2}$$

where ρ is the sea ice density and $U(S,T)$ is the sea ice internal energy per unit mass. The conductivity was determined as the slope of scatter plots of $\rho\partial U/\partial t - (\partial k/\partial z)(\partial T/\partial z)$ vs. $\partial^2 T/\partial z^2$, examples of which are shown in Figure 3.

[15] $U(S,T)$ was found by integrating the heat capacity of *Ono* [1967]. In previous analyses, a typographic error in *Yen* [1981] and *Yen et al.* [1991] was propagated; the correct expression for the heat capacity of sea ice in updated units of J kg^{-1} K^{-1} is $c = 2113 + 7.5 - 3.4\,S + 0.08\,S\theta + 18040\,S/\theta^2$. For each site, measured densities and salinity profiles were used to calculate $U(S,T)$. After low-pass filtering the measured temperatures with a Gaussian window (width 1 day, power spectrum half-height 12 hours) to remove high-frequency components, the derivatives in equation (2) were estimated with centered, second-order, evenly spaced finite difference estimates.Our earlier analysis did not include the second term on the RHS of equation (2). Its inclusion leads to a small reduction in the conductivity, typically less than 3%, and below our experimental scatter (see Figures 3 and 5 in section 4). This term was evaluated through the expansion

$$\frac{\partial k}{\partial z}\frac{\partial T}{\partial z} = \left[\frac{\partial k}{\partial T}\frac{\partial T}{\partial z} + \frac{\partial k}{\partial S}\frac{\partial S}{\partial z}\right]\frac{\partial T}{\partial z} \quad . \tag{3}$$

The spatial derivatives $(\partial T/\partial z)$ and $(\partial S/\partial z)$ are readily calculated from measured temperature and salinity profiles. Values of $(\partial k/\partial T)$ and $(\partial k/\partial S)$ were calculated in a self-consistent fashion using the 'bubbly brine' effective-medium model discussed in section 6. Note that in this step we use only the salinity and temperature sensitivities of the conductivity in that model and not the conductivity values themselves predicted by the model. Physically, these partial derivatives relate to the temperature dependence of the conductivity of pure ice and the equilibrium brine volume fraction, both of which have been measured [*Yen et al.*, 1991]. The temperature dependence (first term on the RHS of equation (3)) is the dominant term here and the predicted variation with temperature is independently supported by the other measurements shown in Figure 7 in section 5. This approach is ultimately justified by the fact that the changes in conductivity due to the inclusion of the second term on the RHS of equation (2) are small, making little difference to the good fit to the experimental conductivities by the 'bubbly brine' effective-medium model.

[16] Calculating the conductivity as the best-fit gradient of the scatter plots of $\rho\partial U/\partial t - (\partial k/\partial z)(\partial T/\partial z)$ versus $\partial^2 T/\partial z^2$ was complicated by the presence of uncertainties in both plotted variables. We calculated k as the geometric mean of linear least squares fits treating each plotted variable as the independent variable; see Figure 3. This returns an unbiased mean if the relative uncertainties are equal for the two variables, but one that is otherwise biased by the difference in these relative errors [*McGuinness et al.*, 1998; *Trodahl et al.*, 2000; *Pringle et al.*, 2006]. Attention must be paid to sampling interval effects which affect the accuracy of the finite difference estimates of $\partial^2 T/\partial z^2$ and $\rho\partial U/\partial t - (\partial k/\partial z)(\partial T/\partial z)$.

[17] We have identified and rectified two effects that contributed to the apparent near-surface reduction in the earlier analysis. Owing to the damping of downward-propagating surface temperature variations, there is always a larger-amplitude high-frequency noise in the $\partial^2 T/\partial z^2$ estimates, calculated from temperatures at three depths, than in the $\rho\partial U/\partial t$ estimates which are calculated from temperatures measured at one depth. We have shown that this can lead to an apparent near-surface conductivity reduction, but that this can be removed by the low-pass filtering implemented here [*Pringle et al.*, 2006]. Secondly, we have identified that pronounced changes in the surface temperature (large rates of change in near-surface temperature and temperature gradient, e.g., near days 235 and 255 in Figure 2a) led to loops in the scatterplots for shallow depths [e.g., *Trodahl et al.*, 2000]. These loops can be understood as Lissajous figures indicating a phase (time) lag between the $\rho\partial U/\partial t - (\partial k/\partial z)(\partial T/\partial z)$ and $\partial^2 T/\partial z^2$ estimates due to sampling intervals that are too coarse for accurate derivative estimates [*Pringle et al.*, 2006]. Both the broadening and decrease in average gradient (principal direction) of these loops reduce the calculated apparent conductivity. Such

loop features clearly indicate nonideal performance of our finite derivative scheme; our analysis is unreliable under these circumstances and we have eliminated periods with such pronounced temperature variations from our analysis.

[18] The salinity gradient in the warm ice near the base of the ice can be both large and time-dependent, and the internal energy $U(S,T)$ is increasingly salinity-dependent at these temperatures. In the absence of real-time in situ salinity measurements over the duration of the measurements, we have therefore excluded temperatures above $-5°C$ from our analysis.

[19] In order to identify the underlying temperature dependence of the conductivity, temperatures were processed in 10- to 15-day blocks, for which we calculated the conductivity and average temperature at the depth of each thermistor. Conductivity values from scatterplots with a goodness of fit parameter $R^2 < 0.9$ were rejected as unreliable. In previous work the apparent increase in conductivity for temperatures above $-9°C$ was interpreted in terms of brine convection enhancing the heat flow, and the accompanying decrease in R^2 values with both depth and increasing temperature gradient identified as possible signatures of non-linear heat flow [*McGuinness et al.*, 1998; *Trodahl et al.*, 2000, 2001]. As our finite difference analysis becomes noise-limited at these depths owing to the attenuation of temperature variations with depth, a decreased R^2 value is actually expected, and either underestimated or overestimated conductivities can result [*Pringle*, 2005]. Temporarily relaxing the $R^2 < 0.9$ and $T < -5°C$ criteria reveals no systematic trend in the apparent conductivity at our sites. Given the uncertainties involved in our finite difference analysis, we conclude that R^2 values alone are an unreliable indicator of convective heat transport.

[20] Any difference between salinity profiles used in our analysis (measured on sampled cores) and the actual instantaneous local salinity leads, through the salinity dependence of the internal energy, to an uncertainty in the calculated conductivity. This uncertainty depends on both salinity and temperature, and for a salinity uncertainty of ±0.5 ppt, typically lies in the range ±(1–5)%. The uncertainty associated with density profiles is approximately ±1%, and in the same sense: underestimating either the salinity or density results in an underestimated conductivity. The sensing position of the thermistors contributes a maximum uncertainty less than 1% that remains constant at each depth.

4. Conductivity Results From Thermistor Arrays in Landfast Ice

[21] We now discuss conductivity results from landfast FY Arctic and Antarctic ice, first assessing accuracy and reproducibility from individual sites, and then calculating temperature-binned average conductivities. Results from two arrays in landfast MY Antarctic ice are also presented.

4.1. Depth and Temperature Dependence in Landfast FY Ice

[22] Our analysis returns a conductivity depth profile. Although crystalline and phase boundary geometries do determine which effective-medium inclusion geometry is most appropriate, and these aspects do depend on depth as well as temperature and salinity, these variations are expected to be smaller than the temperature dependence predicted by effective-medium models. Toward identifying this temperature dependence, we have examined the combined conductivity and average temperature values at each depth from 10- to 15-day periods.

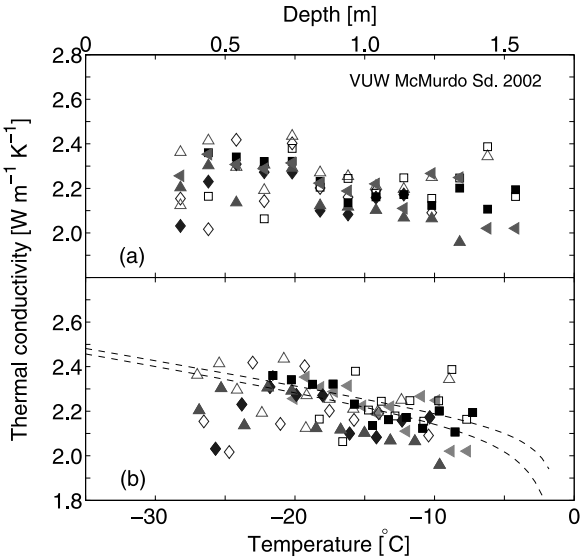

Figure 4. Thermal conductivity results from two VUW arrays 50 m apart in FY landfast ice, McMurdo Sound, 2002. (a) Depth profiles from analysis of temperatures in 10- to 15-day blocks. Open symbols, array MC02(1); solid symbols, MC02(2); different symbols indicate various 10- to 15-day data blocks. (b) The same data as in Figure 4a now plotted against the average temperature at each depth over each period. Dashed lines are 'bubbly brine' effective-medium predictions for $S = 4$ (upper) and 8 (lower) ppt.

[23] In Figure 4 we show the apparent depth- and temperature- dependence of the conductivity from VUW arrays MC02(1) and MC02(2) installed about 50 m apart in FY ice, McMurdo Sound, 2002. The temperature record from array MC02(2) is shown in Figure 2a and the salinity profile measured at the end of the season is shown in Figure 2c along with the profile used in our analysis. Results from arrays MC02(1) and MC02(2) shown by open and solid symbols, respectively, indicate good consistency between the two sites. This is particularly true in the central depths (0.75–1.25 m) where the analysis is more reliable, being neither noise-limited like the lower depths, nor subject to rapid temperature variations like the surface. The scatter derived from the underlying accuracy of the finite difference scheme indicated in Figure 4a is about ±0.15 W m^{-1} K^{-1}, or ±7%. The profiles in Figure 4a suggest a reduction with depth as expected on the basis of the temperature profile. This is explored in Figure 4b which shows the same data plotted against the average temperature at each depth for each 10-day period. The difference between the highest temperatures represented here and the $-5°C$ cut-off is primarily due to the 10-day averaging, but also due to the fact that the scatterplot fits from depths close to the base of the ice (where the temperature variations are weak) did not satisfy $R^2 > 0.9$.

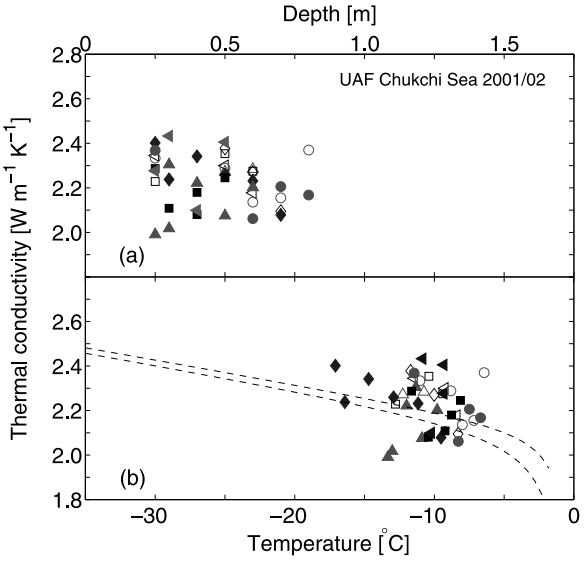

Figure 5. Thermal conductivity results from two UAF arrays in FY landfast ice, Chukchi Sea, near Barrow, Alaska, 2002. (a) Depth profiles from analysis of temperatures in 10- to 15-day blocks. Open symbols, array CS02(1); solid symbols, CS02(2); different symbols indicate various 10- to 15-day data blocks. (b) The same data as Figure 5a now plotted against the average temperature at each depth over each 10-day period. Dashed lines are 'bubbly brine' effective-medium predictions for S = 4 (upper) and 8 (lower) ppt.

[24] These results are centered about the bulk-salinity effective-medium predictions for S = 4 and 8 ppt shown (see section 6). We note that as Figure 4b combines data from all different depths, some scatter is expected on the basis that the data derive from different salinities as well as different temperatures. For example, at −20°C, a 0.04 W m^{-1} K^{-1} lower conductivity is expected for S = 10 ppt than for S = 6 ppt.

[25] Figure 5 shows analogous plots for two UAF sites in the Chukchi Sea, 2002. Here the ice surface temperatures were generally above −20°C and the ice grew to be only 1.35 m thick. The higher scatter in Figure 5a compared with Figure 4a is due to the reduced temperature resolution (δT = 0.02 K) compared with the VUW measurements in Figure 3 ($\delta T = 3 \times 10^{-5}$ K). Optimizing this resolution is discussed in section 8. Figure 5b shows that the apparent temperature dependence is again consistent with predictions. We examine further this temperature dependence with data from other sites and seasons in section 4.2 below. No systematic, anomalous near-surface conductivity reduction is seen at any of the two McMurdo Sound or two Chukchi Sea sites.

4.2. Site and Season Comparison for Arctic and Antarctic FY Ice

[26] To enable a direct comparison of results from different sites and seasons, we have calculated a single arithmetic average conductivity ($\overline{k}$, $\overline{T}$) and standard deviation (σ_k,σ_T) over all depths and temperatures for each array. Here the standard deviation σ_T measures the range in temperatures for which $\overline{k}$ was measured, and σ_k measures the spread in conductivity values. As suggested in Figures 4 and 5 this spread can derive from both measurement scatter and intrinsic temperature dependence over this temperature range. These values are collated in Table 1 and shown in Figure 6, where similar symbols indicate arrays deployed nearby in the same season. Variations in these means of about ±0.05 W m^{-1} K^{-1} might be expected owing to salinity, density and microstructural variations between sites and seasons but overall the mean values agree well within the range at each site. There is excellent agreement between the $\overline{k}$ values from the two UAF sites represented in Figure 5, and between the two VUW sites from Figure 4 and the adjacent UAF site (where a reduced period of data recovery contributed to the large uncertainty in $\overline{k}$ and small temperature range). The four open triangles show values from previously-reported VUW sites after reanalysis. These earlier measurements give somewhat lower values, although the larger sampling time of 60 min at three of these sites reduces the reliability of our finite difference analysis.

[27] Figure 6 shows no clear difference in conductivity values between Antarctic and Arctic FY sites within our experimental resolution. From effective-medium predictions there is no basis to expect such a difference; any small differences due, for example, to the difference in microstructure between thicker frazil ice layers in the Antarctic, or sediment entrainment in landfast Arctic ice, are below our resolution.

4.3. Conductivity Results From Landfast Antarctic MY Ice

[28] The MY results in Figure 6 derive from array measurements in landfast MY ice in Antarctica, 2003. One UAF and one VUW array were installed 100 m apart, in what ice properties and examination of satellite imagery showed to be third-year ice, about 1 km off Arrival Heights near McMurdo Station. The arrays were installed in 4-m-thick ice by the

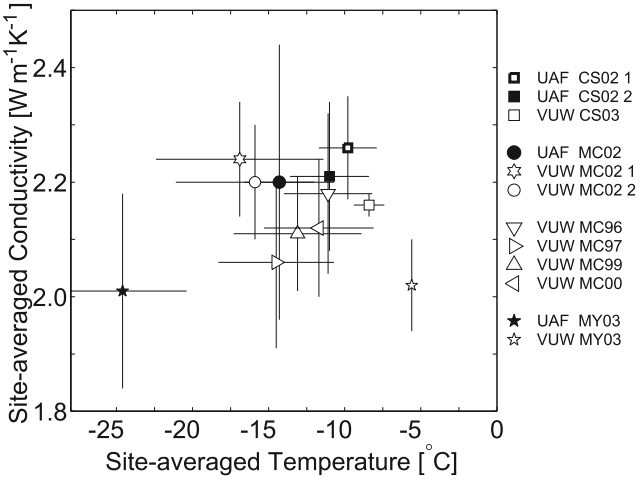

Figure 6. Mean conductivity values for all UAF and VUW arrays against average temperature at landfast FY sites. Error bars are standard deviations in conductivity values and the range of temperatures; see text. Triangles are from previously reported array measurements [*McGuinness et al.*, 1998; *Trodahl et al.*, 2000, 2001], after processing with our amended analysis. The five-sided stars are for landfast MY sites; see section 4.3.

Table 1. Mean and Standard Deviation Thermal Conductivity and Temperature Values, Including Reanalyzed VUW Arrays[a]

	Site (Array)	Δt, min	$\overline{T}$, °C	σ_T, °C	$\overline{k}$, W m^{-1} K^{-1}	σ_k, W m^{-1} K^{-1}	k (Prediction), W m^{-1} K^{-1}
UAF FY	CH02(1)	10	−9.8	1.9	2.26	0.09	2.16 ± 0.07
	CH02(2)	10	−11.0	2.6	2.21	0.13	2.18 ± 0.08
	MC02	30	−14.3	2.3	2.20	0.24	2.22 ± 0.07
VUW FY	MC96[b]	60	−11.1	2.9	2.18	0.14	2.18 ± 0.08
	MC97[b]	60	−14.5	3.8	2.06	0.15	2.22 ± 0.09
	MC99[c]	30	−13.1	4.2	2.11	0.10	2.22 ± 0.10
	MC00	60	−11.7	3.6	2.12	0.12	2.19 ± 0.09
	MC02(1)	30	−16.9	5.5	2.24	0.10	2.25 ± 0.11
	MC02(2)	30	−15.9	5.2	2.20	0.10	2.24 ± 0.11
	CH03	30	−8.4	1.0	2.16	0.02	2.13 ± 0.06
UAF MY	MC03	30	−24.6	4.2	2.01	0.17	2.05 ± 0.11
VUW MY	MC03	30	−5.6	0.2	2.02	0.08	1.93 ± 0.08

[a]Site names indicate location (CH is Chukchi Sea, MC is McMurdo Sound) and year. The last column is the effective-medium prediction for the given temperature range and average salinity and densities at these sites using our 'bubbly brine' model for the FY ice, and the 'bubbly ice' model of [*Schwerdtfeger*, 1963] for MY ice.
[b]Earlier analysis published by *Trodahl et al.* [2000].
[c]Earlier analysis published by *Trodahl et al.* [2001]

refreezing of 2-m-deep auger holes. Low-salinity water was poured into these holes so that the salinity of the refrozen ice approximately matched that of the surrounding ice. In this area the surface ice was bubbly but otherwise very clear, with a low density (820 ± 20 kg m^{-3}) and salinity (0.2 ± 0.2 ppt) suggesting a refrozen melt layer.

[29] Table 1 shows that the lower MY conductivity values in Figure 6 are consistent with the expected density dependence. No anomalous surface reduction was observed in the depth profiles from these sites. These landfast results are not representative of MY ice in general, which, due to deformation and thermodynamic cycling, can exhibit high variability in density, salinity and microstructure [e.g., *Eicken et al.*, 1995], but they do serve to emphasize the strong density dependence of the conductivity, $k \lesssim \rho$, which is not addressed in equation (1).

5. Comparison With Effective-Medium Predictions and Modelers' Representation

[30] To compare our FY results with the modeling parameterization and effective-medium predictions we have temperature-binned data from the following Antarctic and Arctic arrays: (MC99, MC00, MC02(1,2); CS02(1,2)). These sites were least affected by data collection interruptions, had measurement intervals not greater than 30 min (except MC00 for which the high temperature resolution of the custom built logger provides some compensation) and had well-characterized salinity profiles. Average conductivity and temperatures calculated in this way are collated in Table 2 and shown in Figure 7 together with several historical measurements discussed below and our recent direct measurements on surface and subsurface FY McMurdo Sound sea ice [*Pringle et al.*, 2006]. Also shown are the predictions for S = 4 and 8 ppt of the *Maykut and Untersteiner* [1971] parameterization and an effective-medium model considering the parallel flow of heat along ice and 'bubbly brine' components (see section 6).

[31] The direct comparison of our measured and predicted values in Figure 7 is again complicated by the temperature-binned results deriving from different sites and depths and therefore different salinity and density values. It is nevertheless quite clear that the effective medium predictions provide a better fit to our data than the parameterization of *Maykut and Untersteiner* [1971]. This match is best between −10°C and −25°C where most of our measurements lie. The few lower temperature results derive largely from the high-salinity surface at just two sites. Their departure from predicted values is not significant and certainly not comparable to the anomalously low values previously found systematically over the top 50 cm. In excluding temperatures above −5°C, we lack results where the predicted conductivity decrease is strongest. Nevertheless, the present results show no sign of the strong conductivity increase above −9°C previously associated with a convective enhancement to the heat flow [*Trodahl et al.*, 2001].

[32] The higher temperature range is covered by several of the historical measurements collated in Table 3. Where there are temperature overlaps, they are generally consistent with ours. The laboratory measurements on artificial sea ice

Table 2. Temperature-Binned Average Conductivity Values for FY Sea Ice, Chukchi Sea (UAF and VUW), and McMurdo Sound (VUW)[a]

k, W m^{-1} K^{-1}	σ_k, W m^{-1} K^{-1}	T, °C	σ_T, °C
	Chukchi Sea		
2.33	0.08	−16.0	1.2
2.15	0.14	−12.9	0.4
2.27	0.11	−11.0	0.6
2.21	0.10	−9.0	0.5
2.21	0.09	−7.2	0.6
	McMurdo Sound		
2.24	0.11	−26.8	0.2
2.21	0.18	−25.1	0.6
2.24	0.12	−23.2	0.6
2.30	0.08	−21.0	0.7
2.35	0.08	−19.3	0.3
2.25	0.09	−18.8	0.6
2.16	0.13	−17.0	0.6
2.19	0.08	−15.0	0.7
2.15	0.09	−12.9	0.7
2.13	0.15	−10.9	0.5
2.20	0.13	−9.1	0.5
2.14	0.09	−7.1	0.6

[a]Uncertainties are standard deviations for k and T in each bin. Bins have at least n = 4 measurements and are no smaller than 2°C wide.

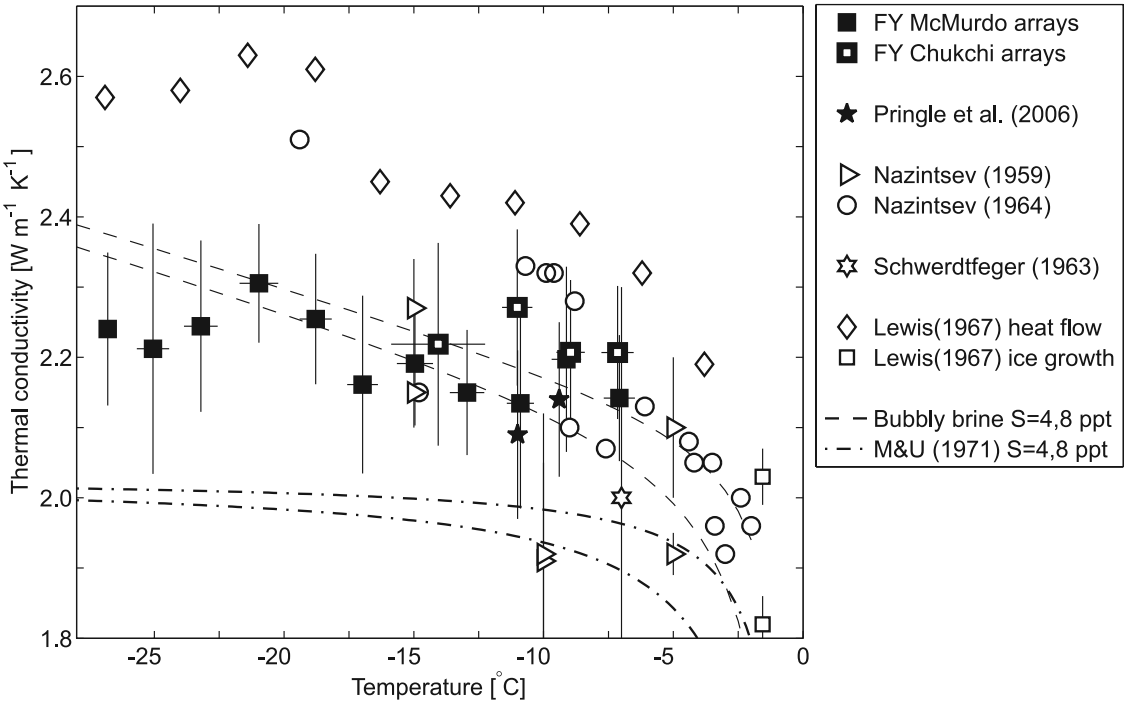

Figure 7. Present and previous conductivity results compared with values predicted by *Maykut and Untersteiner* [1971] parameterization for $S = 4$, 8 ppt (dash-dotted lines), and our 'bubbly brine' effective-medium model for $S = 4$, 8 ppt (dashed lines); lower curve is 4 ppt in both cases. Solid squares and thick-lined squares are temperature-binned conductivity averages from landfast FY ice in McMurdo Sd. and the Chukchi Sea, respectively. Stars are our recent direct measurements *[Pringle et al.*, 2006]. Open symbols from labeled historical measurements; see section 5 and Table 3.

samples of *Nazintsev* [1964] in particular show the predicted conductivity decrease with increasing brine volume. These laboratory measurements are not subject to the problem of the accurately measuring salinity profiles near the base of the ice, which affects temperature array-based methods. Of the results for $T > -5$°C in Figure 7, only those of *Lewis* [1967] are derived from array measurements.

[33] The somewhat-higher values from *Lewis* [1967] derived from his so-called 'monochromatic' heat flow analysis in which it was assumed that all heat is transported with no dispersion by the dominant frequency component of the surface temperature variation. This analysis also used a constant oceanic heat flux calculated from the measured seasonal change in the water column temperature. *Lewis* [1967] also used this Oceanic heat flux to calculate the conductivity at the ice/ocean interface from the rate of ice growth. *Schwerdtfeger* [1963] measured the ratio of temperature gradients in a block of pure ice and the FY ice cover it was frozen into. *Nazintsev* [1964] measured the conductivity of artificial sea ice samples [see also *Doronin and Kheisin*, 1977], as well as the heat capacity and thermal diffusivity of natural sea ice samples [*Nazintsev*, 1959] from which we have calculated conductivity values using $\rho = 910$ kg m^{-3}.

6. A Proposed Conductivity Parameterization Derived From Effective-Medium Models

[34] The results in Figure 7, particularly those at colder temperatures, are about 10–15% higher than the parameterization of *Maykut and Untersteiner* [1971]. This difference is not entirely unexpected in that the latter were concerned primarily with multi-year sea ice, which typically exhibits higher gas volume fractions and therefore lower densities, at least in the upper layers of the ice cover [*Eicken et al.*, 1995]. However, common practice has been to employ the same parameterization equally to first-year ice, or areas with a significant and/or increasing fraction of FY ice, for which Figure 7 suggests this approach is not valid. We now describe an alternative expression for the conductivity derived by considering effective medium models appropriate to MY and FY ice.

[35] The effective-medium model of *Schwerdtfeger* [1963] considers parallel heat flow along brine and 'bubbly ice'. While this bubbly ice picture is appropriate for MY ice, recent work shows that in FY ice, air bubbles are almost entirely found within brine inclusions [*Light et al.*, 2003]. With this in mind, we have examined an analogous 'bubbly brine' model. Owing to the expressions for thermal equilibrium volume fractions these models do not provides a simple analytical expression for $k(\rho, S, T)$, even if the mixing formula applied to the bubbly phase is simplified [e.g., *Ono*, 1967]. Our approach has been to fit simple analytical expressions to the output of both the bubbly ice and bubbly brine models. We have found that both models can be well represented by a single expression for the appropriate density and salinity ranges.

[36] Details of the models are as follows. In units of W m^{-1} K^{-1}, we have used $k_i = 2.14 - 0.011\theta$, derived from

Table 3. Previous Measurements of Sea Ice Thermal Conductivity Shown in and Outlined in Section 5

Reference	Type	ρ, kg m^{-3}	S ppt	Depth, m	$k \pm \Delta k$, W K^{-1}	m^{-1}	T, °C
Pringle et al.	FY	900	5.3	0–0.1	2.14	0.11	−9.4
[2006][a]	FY	920	4.5	0.4–0.5	2.09	0.11	−11.0
	MY	820	0.2	0–0.1	1.88	0.13	−13.0
Lewis [1967][b]	FY	915	5	1.65	2.03	0.04	−1.57
					1.69	0.04	−1.57
					1.82	0.04	−1.57
Lewis [1967][c]	FY	915	1.8	0.00	2.62	-	−30.9
			1.2	0.15	2.57		−26.9
			0.6	0.30	2.58		−24
			0.5	0.45	2.63		−21.4
			0.9	0.60	2.61		−18.8
			1.4	0.75	2.45		−16.3
			1.9	0.90	2.43		−13.6
			2.4	1.05	2.42		−11.1
			2.9	1.20	2.39		−8.6
			3.4	1.35	2.32		−6.2
			3.9	1.50	2.19		−3.8
			4.5	1.65	2.03		−1.6
Schwerdtfeger [1963][d]	FY	910	6	0–0.3	2.1	0.3	−7.0
Nazintsev [1959][e]	FY		3.59	0.1	2.10	0.10	−5
					1.91	0.21	−10
					2.27	0.07	−15
	FY		3.86	1.7	1.92	0.03	−5
					1.92	0.13	−10
					2.15	0.05	−15
Nazintsev [1964][f]	Lab.	906	3.85	-	2.05	-	−3.5
		906			2.08		−4.4
		906			2.28		−8.8
		906			2.32		−9.6
		906	4.7	-	1.96	-	−2.0
		906			2.00		−2.4
		906			1.92		−3.0
		904			1.96		−3.4
		908			2.05		−4.2
		904			2.13		−6.1
		906			2.07		−7.6
		904			2.10		−9.0
		904			2.32		−9.9
		906			2.33		−10.7
		904			2.15		−14.8
		904			2.51		−19.4

[a]Density ±10 kg m^{-1}, salinity ±0.2 ppt.
[b]From ice/water interface growth, ρ value assumed not measured.
[c]Monochromatic heat flow analysis, ρ value assumed not measured.
[d]Ratio of FY and fresh ice temperature gradients.
[e]Calculated from reported measurements of heat capacity and thermal diffusivity with ρ = 910 kg m^{-3}.
[f]Results also listed by *Doronin and Kheisin* [1977]. The results of *Malmgren* [1927] and *Weller* [1967] were excluded as unreliable.

the 'best estimate' values of *Slack* [1980] [see also *Lide*, 2005] based on compiled measurements. The conductivity of the bubbly phase was found with the Maxwell mixing formula and temperature-dependent thermal equilibrium ice, brine and air volume fractions calculated for input salinity and density [*Yen*, 1981; *Yen et al.*, 1991]. Although these volume fraction relations have been derived under the assumption of no salt precipitation, and are strictly valid only for $T > -8$ °C, the precipitate volume fraction is only of the order of 1% even at −30°C [*Assur*, 1958], so applying them for $T > -30$°C introduces an uncertainty smaller than that arising from the component conductivities. We used $k_b = 0.523 + 0.013\theta$ [*Lange and Forke*, 1952] and $k_a = 0.025$ [*Yen*, 1981] for the brine and air components, respectively. Of the required parameters, the conductivity of pure ice at 0 °C is the least accurately known, with values ranging from 2.09 to 2.23 W m^{-1} K^{-1} [*Fukusako*, 1990].

[37] We first consider the original bubbly ice model of *Schwerdtfeger* [1963] over the density and salinity ranges $840 < \rho < 940$ kg m^{-3}, $0 < S < 10$ ppt, and for -30°C $< \theta < -1.8$°C. For these conditions, which span almost all sea ice conditions, we have found the full model output is well approximated by

$$k = \frac{\rho}{\rho_i}\left(2.11 - 0.011\,\theta + 0.09\,\frac{S}{\theta} - \frac{(\rho - \rho_i)}{1000}\right) \quad , \qquad (4)$$

where $\rho_i = 917$ kg m^{-3} is the density of pure ice. Figure 8a illustrates the goodness of fit for representative salinity and density values. The functional form of equation (4) was chosen to capture the first-order temperature dependence of the component conductivities and the brine volume contribution, and to account for the essentially negligible conductivity of the air volume fraction. The coefficients were obtained by examining the residuals shown in Figure 8. This process was simplified in that the overall magnitude, temperature dependence, behavior above −5°C, and density scaling of the residuals are each primarily controlled by the coefficient of only one term in equation (4). The sign of the last term might seem to imply an increased conductivity for low-density ice, but this term is only a correction to the main density dependence in the prefactor. Over the parameter range considered, equation (4) reproduces the full model behavior to within an error of ±2% which is less than the model uncertainty derived from the component conductivities, so any precision in these coefficients higher than that given is probably not justified.

[38] We now consider the bubbly brine model for densities appropriate to FY ice, $\rho = 890 - 930$ kg m^{-3}. Because the air volume now reduces the conductivity of the lower conductivity brine rather than the ice, the bubbly brine

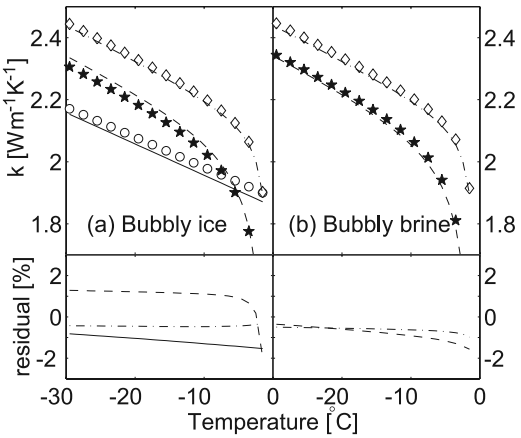

Figure 8. Comparison of conductivity values predicted by equation (4) (lines) with the effective-medium predictions (symbols) from (a) the *Schwerdtfeger* [1963] 'bubbly ice' model, and (b) our 'bubbly brine' model. In both cases circles and solid line are for ρ = 840 kg m^{-3}, S = 0 ppt; stars and dashed line are for ρ = 909 kg m^{-3}, S = 12 ppt; and diamonds and dash-dotted line are for ρ = 920 kg m^{-3}, S = 4 ppt. The bottom plots show the fractional residuals.

model returns a conductivity higher than the bubbly ice model. This difference increases as density decreases, but as evident in comparing Figures 8a and 8b, is small for densities relevant to FY ice. Equation (4) provides a good fit to the output of both models over the density ranges for which they are each physically appropriate, and therefore provides a single expression applicable to both MY and FY ice. When $\rho \approx \rho_i$, the last term in equation (4) is small, and for $\rho \gtrsim 890$ kg m^{-3}, the simpler expression found by dropping this term,

$$k = \frac{\rho}{\rho_i}\left(2.11 - 0.011\,\theta + 0.09\,\frac{S}{\theta}\right) \quad , \tag{5}$$

fits both models to within ±2%. As a point of difference with the MU parameterization, equations (4) and (5) both require the user to specify sea ice density in addition to salinity and temperature.

[39] Our array results derive from landfast, undeformed FY ice, typically with a salinity of 5–6 ppt and density 900 – 920 kg m^{-3}. Further to being consistent with these results, equations (4) and (5) are more generally applicable because they have been derived to reproduce the density, salinity and temperature dependence of the effective-medium models considered above; the appropriate one of which (bubbly ice) is also consistent with our Antarctic MY results from array measurements (see Table 2) and direct measurements [*Pringle et al.*, 2006].

[40] To briefly assess the difference in total heat flow using equations (1), (4), and (5), consider a nondivergent heat flux ($J_Q = k\nabla T$ constant with depth) through snow-free 2-m-thick MY ice with an upper surface temperature of −15°C and a base temperature −1.8°C. Following the Community Climate System Model (CCSM3.0) we use a constant density, ρ = 900 kg m^{-3}, and a vertical salinity profile varying from 0 at the surface to 3.2 ppt at the ice water interface according to $S(w) = 1.6(1 - \cos(\pi w^{(0.407/0.573+w)})$, where $w = z/h$ is the normalized height [*Briegleb et al.*, 2004]. In this case the surface thermal conductivity given by equations (1), (4), and (5) is 2.03, 2.25, 2.23 W m^{-1} K^{-1}, respectively, and the depth-averaged conductivity is 1.95, 2.14, 2.12 W m^{-1} K^{-1}, respectively. For a similarly simplified representation of FY ice, we take a constant salinity of 6 ppt, and constant density of 920 kg m^{-3}. In this case the surface conductivity for the same temperature profile is 1.98, 2.24, 2.25 W m^{-1} K^{-1}, respectively, and the depth-averaged conductivity is 1.91, 2.12, 2.12 W m^{-1} K^{-1}, respectively. The associated nondivergent heat fluxes found using either equation (4) or (5) are approximately 8% and 11% higher than the MU parameterization for these model-like representations of MY and FY ice, respectively. If, as more appropriate for wintertime Antarctic conditions, the surface temperatures is −30°C then the total heat flux difference for the FY case increases to 15%.

7. Convective Events: Thermal Signatures and Heat Flow Contribution

[41] Thermal signatures associated with internal brine motion, or so-called 'convective events' were recorded in some, but not all, of the earlier temperature records

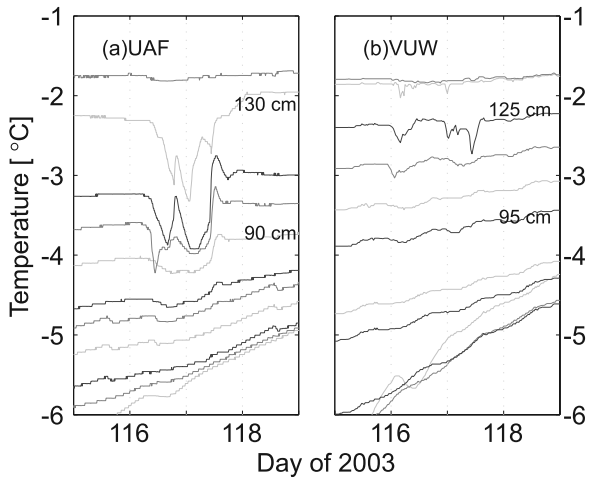

Figure 9. Thermal signatures attributed to convective events recorded in (a) UAF and (b) VUW arrays separated by 100 m, Chukchi Sea, 2003. Day 116 is 26 April. For both arrays, thermistor spacings are Δz = 10 cm, although there are gaps where thermistors failed. These events followed the first strong surface warming of the year, and no other events were observed at these sites.

[*McGuinness et al.*, 1998; *Trodahl et al.*, 2000, 2001]. Over 15 Antarctic and Arctic array measurements (including three not analyzed here owing to measurement problems which nonetheless did not prevent the identification of convective events) we observed 22 distinct events in 1957 days of measurements. Of the eight arrays that did register events, the average occurrence was 2.75 events in 4.5 months. These fell into two populations: those occurring near the base of the ice during winter growth, and those late in the season. The former were usually recorded by the lowest 25 cm in the ice, whereas the latter could extend over up to 80 cm in the ice interior. Figure 9 shows examples of the latter type, recorded simultaneously by UAF and VUW arrays 100 m apart in the Chukchi Sea near Pt. Barrow, Alaska, 2003. The UAF site also included an array of dielectric probes, sensitive to changes in the in situ brine content and salinity, which also recorded these events [*Backstrom and Eicken*, 2006]. This event immediately followed the first sustained surface warming of the season. We believe that this sufficiently increased the volume fraction, and thereby the connectivity and permeability, of the brine volume in the upper layers of the ice to enable a discharge of this head of dense, cold saline brine through an already well-connected brine network below (H. Eicken et al., manuscript in preparation, 2007). This interpretation is supported by the direction of the temperature variation: an initial cooling followed by warming, associated with both sensible and latent heat release, as the brine reequilibrates.

[42] The heat flow associated with brine motion in sea ice, whether drainage of a brine channel or network, or an inflow of sea water into a drained channel, is largely a latent heat flux. *Trodahl et al.* [2000] pointed out the salt flux associated with a 10% enhancement to winter heat flow through brine drainage would lead to unphysically high desalination rates that would drain the ice in less than a

season. Here we estimate the maximum heat flow associated with the refreezing of an influx of sea water into a drained brine channel. In particular, we consider spring conditions, for which large drainage features can be characterized by 1-cm-diameter channels with 15-cm lateral separations (Miner et al., manuscript in preparation, 2007).

[43] For a cylindrical brine tube of constant radius r, and height h, the latent heat Q_L delivered to the ice is given by

$$Q_L = \int_0^h \rho\pi r^2 L(S,\theta)dz \quad . \tag{6}$$

Here S and $L(S,\theta) = 4.187\ (79.68 - 0.505\ \theta - 0.0273\ S + 4.3115\ S/\theta + 0.0008\ S - 0.0009\theta^2)$ is the heat released by the growth of sea ice of salinity S (ppt) at temperature θ, both of which are functions of height z above the base of the ice. This expression derives from *Ono* [1967]; note that the last term is incorrectly given as a factor of 10 too large in the review articles of *Yen* [1981] and *Yen et al.* [1991].

[44] Taking $h = 0.8$ m and an upper temperature of -6°C as in the event shown in Figure 9, using $r = 0.5$ cm, freezing to the surrounding salinity profile, and including the smaller sensible heat term, we find a total heat release of 80 kJ. Note that as this calculation simply assumes complete freezing of the channel, the same result holds whether this occurs in a single event or gradually through a repeated cycle of convective overturning causing incremental freezing, for example, driven by a density instability [*Martin*, 1970; *Eide and Martin*, 1975; *Niedrauer and Martin*, 1979].

[45] A brine channel spacing of 15 cm gives a heat flow of approximately 3.5 MJ m^{-2}. This corresponds to the heat released by the growth of about 3 cm of new basal ice or 2 days of conductive heat flow up the ice for a temperature gradient of 10 K m^{-1}. Therefore the heat flow associated with such events in winter/spring ice is of the order of a few percent of the total winter heat flux.

[46] The nature of our thermistor measurements does not allow us to assess the magnitude of convective heat transfer associated with brine overturning in the highly permeable, lowermost ice layers. Laboratory work and field measurements indicate that this process is most pronounced in the bottom 5 to at most 10 cm of a first-year ice cover [*Notz et al.*, 2005; Miner et al., manuscript in preparation, 2007].

8. Comments on Thermistor Strings and Temperature Measurement

[47] The results of section 4.2 in particular indicate differences in the design of the VUW and UAF thermistor string designs had no significant effect on the calculated conductivity. It is likely that the most accurate future measurements could be made by combining the attention to conductance matching in the VUW arrays with the 'protruding finger' design of the UAF arrays. However, it is the measurement precision (temperature resolution) that affects the accuracy of the finite difference analysis presented here, which is ultimately limited by the analog to digital converter (ADC) in the data logger. This can however be optimized in the measurement circuitry (e.g., reference resistors in bridge circuits), and by averaging multiple (e.g., n = 10 – 20) quickly repeated measurements for each reading, thereby decreasing the sampling error by a factor of $n^{1/2}$ and potentially reducing the ADC-limited discretization. Our experience indicated that combining these steps could reduce the discretization in temperatures measured with CR10X loggers by more than an order of magnitude [*Pringle*, 2005]. The accuracy of the time derivatives can be further improved by reducing time sampling intervals to 10 or 15 min to enable smoothing before derivative estimation.

9. Conclusions

[48] We have presented thermal conductivity results from an amended analysis of several seasons of in situ temperature measurements in landfast Antarctic and Arctic sea ice. This follows a careful reassessment of the analysis applied to earlier measurements, which showed that both an anomalous, strong near-surface conductivity reduction and an apparent conductivity increase above -9°C were data-processing artifacts. Neither result is observed following our amended analysis. Data processed in 10- to 15-day periods indicate that our graphical finite difference derivative analysis has an accuracy of about ±0.15 W m^{-1} K^{-1} (±7%). Direct comparison of results from different sites and seasons is somewhat complicated by variations in ice structure, salinity and density. Nevertheless, within this level of accuracy our results from landfast FY ice show good reproducibility between neighboring sites, and no significant difference between ice in McMurdo Sound, Antarctica and in the Chukchi Sea off Barrow, Alaska. They are also consistent with recent direct measurements on landfast McMurdo Sound FY ice [*Pringle et al.*, 2006]. Differences between the two array designs used were not important as regards the calculated conductivity, but attention to both temperature measurement resolution and sampling interval effects was important.

[49] Temperature-binned results from FY ice and reliable historical measurements are in agreement with the effective-medium predictions, particularly between -25°C and -10°C, but 10–15% higher than the commonly used modelers' parameterization of *Maykut and Untersteiner* [1971]. This parameterization was derived for Arctic multi-year ice but is commonly applied also in large-scale models of Antarctic and Arctic first-year ice. Particularly in the Antarctic, with its colder temperatures and larger FY cover, our results show this to be inappropriate.

[50] On the basis of the good agreement of the effective-medium predictions with both our experimental results for FY and MY ice and the other results shown in Figure 7, we propose an alternative parameterization that is applicable to both FY and MY, landfast and pack ice. We considered 'bubbly ice' and 'bubbly brine' effective medium models to represent MY and FY ice in the temperature range -30°C < θ < -1.8°C. The density, salinity and temperature dependence of model output over the appropriate density range for both models is reproduced to within ±2% by $k = (\rho/\rho_i)(2.11 - 0.011\ \theta + 0.09\ S/\theta + (\rho - \rho_i)/1000)$. In a similar vein to that in which the *Maykut and Untersteiner* [1971] expression was proposed, this expression both captures the dominant features of effective model predictions and is consistent with experimental results. The ±2% accuracy is within the underlying model uncertainties arising from the uncertainty in the conductivity of pure ice. As this uncer-

tainty is reduced, the coefficients in equation (2) may need to be refined accordingly. For $\rho \gtrsim 890$ kg m^{-3} this expression can be simplified by dropping the last term. The two key points of difference between our representation and that of *Maykut and Untersteiner* [1971], is that ours is applicable to both FY and MY ice, but to do so requires the user to specify density.

[51] The difference in steady-state heat flux from our proposed parameterization and that of *Maykut and Untersteiner* [1971] for model-like representations of MY and FY ice is approximately 5–10% and 5–15%, respectively. Support for our proposed parameterization is provided by this difference, its comparison with the larger and more accurate currently available experimental data set, and its more general applicability derived from its foundation on suitably modified and updated effective-medium models. By virtue of its derivation from effective-medium models, this expression is in principle also applicable to brackish, lake and glacial ice for specified density, salinity and temperature.

[52] In 1957 days of combined Arctic and Antarctic measurements during winter and early spring measurements, we observed 22 events showing thermal signatures of internal brine motion. From the latent heat flux released with the refreezing of 80-cm-tall, 1-cm-diameter channels, 15 cm apart, we estimate a contribution to the heat flow of the order of several percent over this period. This maximum contribution assumes one such full freezing per channel per season, which is likely to occur in the spring.

Notation

c	heat capacity, J kg^{-1} K^{-1}.
k	thermal conductivity, W m^{-1} K^{-1}.
ρ	density, kg m^{-3}.
ρ_i	density of pure ice, 917 kg m^{-3}.
S	salinity, ppt.
T	temperature.
θ	temperature, for values in Celsius, ° C.
U	internal energy per unit mass, J kg^{-1}.

Subscripts

i	ice.
b	brine.
a	air.
no subscript	sea ice.

For practical purposes, the nondimensional practical salinity unit (psu) scale used for ocean water, and the gravimetric ppt unit, representing relative mass fraction of dissolved salts in parts per thousand, are interchangeable for the range 1 – 42 ppt/psu [*Eicken*, 2003]. Presently, some sea ice models refer to salinity in psu, and others in ppt. The equations in this paper can be used with S in either unit.

[53] **Acknowledgments.** We acknowledge with sadness the contribution to this work of Karoline Frey, who died in a crevasse fall on 24 March 2002. We gratefully acknowledge the technical and field support of Tim Haskell, Alan Rennie, Dave Gilmour, Andy Mahoney, Craig Zubris, and Meg Smith, and discussions with Mark McGuinness and Ken Golden. Logistics and field support in Antarctica was provided by Antarctica New Zealand and Raytheon, and in Barrow by the Barrow Arctic Science Consortium (BASC). This work was funded by the New Zealand Public Good Science Fund and by NSF (OPP 0126007). Any opinions, findings, and conclusions or recommendations expressed in this material are those of the authors and do not necessarily reflect the views of the National Science Foundation.

References

Anderson, D. L. (1958), A model for determining sea ice properties, in *Arctic Sea Ice*, Publ. 598, pp. 148–152, Natl. Acad. Press, Washington, D. C.

Assur, A. (1958), Composition of sea ice and its tensile strength, in *Arctic Sea Ice*, Publ. 598, pp. 106–138, Natl. Acad. Press, Washington, D. C.

Backstrom, L. G. E., and H. Eicken (2006), Capacitance probe measurements of brine volume and bulk salinity in first-year sea ice, *Cold Reg., Sci. Technol.*, *46*(1), 167–180, doi:10.1016/j.coldregions.2006.08.018.

Briegleb, B. P., C. M. Bitz, E. C. Hunke, W. H. Lipscomb, M. M. Holland, J. L. Schramm, and R. E. Moritz (2004), Scientific description of the sea ice component in the Community Climate System Model, version 3, *NCAR/TN-463+STR*, 70 pp., Natl. Cent. for Atmos. Res., Boulder, Colo.

Dieckmann, G. S., and H. H. Hellmer (2003), The importance of sea ice: An overview, in *Sea Ice—An Introduction to its Physics*, *Biology, Chemistry and Geology*, edited by D. N. Thomas and G. S. Dieckmann, pp. 1–21, Blackwell Sci., Malden, Mass.

Doronin, Y. P., and D. E. Kheisin (1977), *Sea Ice*, translated from Russian, Amerind, New Delhi.

Eicken, H. (2003), From the microscopic to the macroscopic to the regional scale: Growth, microstructure and properties of sea ice, in *Sea Ice—An Introduction to its Physics*, *Biology, Chemistry and Geology*, edited by D. N. Thomas and G. S. Dieckmann, pp. 22–81, Blackwell Sci., Malden, Mass.

Eicken, H., M. Lensu, M. Leppranta, W. B. Tucker III, A. J. Gow, and O. Salmela (1995), Thickness, structure and properties of level summer multiyear ice in the Eurasian sector of the Arctic Ocean, *J. Geophys. Res.*, *100*, 22,697–22,710.

Eide, L., and S. Martin (1975), The formation of brine drainage features in young sea ice, *J. Glaciol.*, *14*, 137–154.

Fichefet, T., and M. M. Maqueda (1997), Sensitivity of a global sea ice model to the treatment of ice thermodynamics and dynamics, *J. Geophys. Res.*, *102*, 12,609–12,646.

Frey, K., H. Eicken, D. Perovich, T. C. Grenfell, B. Light, L. H. Shapiro, and A. P. Stierle (2001), Heat budget and decay of clean and sediment-laden sea ice off the northern coast of Alaska, paper presented at Port and Ocean Engineering in the Arctic Conference (POAC '01), Port and Ocean Eng. Under Arctic Cond., Ottawa, Ont., Canada.

Fukusako, S. (1990), Thermophysical properties of ice, snow and sea ice, *Int. J. Thermophys.*, *11*(2), 353–373.

Lange, N. A., and G. M. Forke (1952), *Handbook of Chemistry*, 8th ed., Handbook Publ., Sandusky, Ohio.

Lemke, P., W. Owens, and W. D. Hibler III (1990), A coupled sea ice–mixed layer–pycnocline model for the Weddell Sea, *J. Geophys. Res.*, *95*, 9513–9525.

Lewis, E. L. (1967), Heat flow through winter ice, in *Physics of Snow and Ice: International Conference on Low Temperature Science 1966*, vol. 1 (1), edited by H. Oura, pp. 611–631, Inst. of Low Temp. Sci., Hokkaido Univ., Sapporo, Japan.

Lide, R. T., (Ed.) (2005), *Handbook of Chemistry and Physics*, 85th ed., CRC Press, Boca Raton, Fla.

Light, B., G. A. Maykut, and T. C. Grenfell (2003), Effects of temperature on the microstructure of first-year Arctic sea ice, *J. Geophys. Res.*, *108*(C2), 3051, doi:10.1029/2001JC000887.

Malmgren, F. (1927), On the properties of sea ice, in *The Norwegian North Polar Expedition with the "Maud', 1918–1925*, vol. 1, Part 5, pp. 1–67, Geofys. Inst., Bergen, Norway.

Martin, S. (1970), A hydrodynamic curiosity: The salt oscillator, *Geophys. Fluid Dyn.*, *1*, 143–160.

Maykut, G., and N. Untersteiner (1971), Some results from a time-dependent thermodynamic model of sea ice, *J. Geophys. Res.*, *76*, 1550–1576.

McGuinness, M. J., K. Collins, H. J. Trodahl, and T. G. Haskell (1998), Nonlinear thermal transport and brine convection in first year sea ice, *Ann. Glaciol.*, *27*, 471–476.

Nazintsev, Y. L. (1959), Eksperimental'noe opredelenie teploemkosti i temperaturoprovodnosti moskogo l'da (Experimental determination of the specific heat and thermometric conductivity of sea ice), *Probl. Arkt. Antarkt.*, *1*, 65–71, (English translation available from Am. Meterol. Soc., Boston, Mass.)

Nazintsev, Y. L. (1964), Nekotorye dannye k raschetu teplovykh Svoistv morskogo l'da. (Some data on the calculation of thermal properties of sea ice), *Tr. Arkt. Antarkt. Nauchlo Issled Inst.*, *267*, 31–47.

Niedrauer, T., and S. Martin (1979), An experimental study of brine drainage and convection in young sea ice, *J. Geophys. Res.*, *84*, 1176–1186.

Notz, D., J. S. Wettlaufer, and M. G. Worster (2005), A non-destructive method for measuring salinity and solid fraction of growing sea ice in situ, *J. Glaciol.*, *51*, 159–166.

Ono, N. (1967), Specific heat and fusion of sea ice, in *Physics of Snow and Ice: International Conference on Low Temperature Science 1966*, vol. 1 (1), edited by H. Oura, pp. 599–610, Inst. of Low Temp. Sci., Hokkaido Univ., Sapporo, Japan.

Parkinson, C., and W. Washington (1979), A large-scale numerical model of sea ice, *J. Geophys. Res.*, *84*, 311–337.

Pringle, D. J. (2005), Thermal conductivity of sea ice and Antarctic permafrost, Ph.D. thesis, Victoria Univ. of Wellington, Wellington, N. Z.

Pringle, D. J., H. Trodahl, and T. Haskell (2006), Direct measurement of sea ice thermal conductivity: No surface reduction, *J. Geophys. Res.*, *111*, C05020, doi:10.1029/2005JC002990.

Schwerdtfeger, P. (1963), The thermal properties of sea ice, *J. Glaciol.*, *4*, 789–807.

Slack, G. A. (1980), Thermal conductivity of ice, *Phys. Rev. B*, *22*(6), 3065–3071.

Trodahl, H. J., M. McGuinness, P. Langhorne, K. Collins, A. Pantoja, I. Smith, and T. Haskell (2000), Heat transport in McMurdo Sound first-year fast ice, *J. Geophys. Res.*, *105*, 11,347–11,358.

Trodahl, H. J., S. Wilkinson, M. McGuinness, and T. Haskell (2001), Thermal conductivity of sea ice: Dependence on temperature and depth, *Geophys. Res. Lett.*, *28*, 1279–1282.

Untersteiner, N. (1961), On the mass and heat balance of Arctic sea ice, *Arch. Meteorol. Geophys. Bioklimatol., Ser. A*, *12*, 151–182.

Vancoppenolle, M., T. Fichefet, and C. M. Bitz (2005), On the sensitivity of undeformed Arctic sea ice to its vertical salinity profile, *Geophys. Res. Lett.*, *32*, L16502, doi:10.1029/2005GL023427.

Vancoppenolle, M., C. M. Bitz, and T. Fichefet (2007), Summer landfast sea ice desalination at Point Barrow, Alaska: Modeling and observations, *J. Geophys. Res.*, doi:10.1029/2006JC003493, in press.

Weller, G. (1967), The effect of absorbed solar radiation on the thermal diffusion in Antarctic fresh-water ice and sea ice, *J. Glaciol.*, *6*, 859–878.

Wettlaufer, J. (1991), Heat flux at the ice-ocean interface, *J. Geophys. Res.*, *96*, 7215–7236.

Wu, X., I. Simmonds, and W. Budd (1997), Modeling of Antarctic sea ice in a general circulation model, *J. Clim.*, *10*(4), 593–609.

Yen, Y.-C. (1981), Review of thermal properties of snow, ice and sea ice, *Rep. 81–10*, U. S. Army Cold Reg. Res. and Eng. Lab., Hanover, N. H.

Yen, Y.-C., K. C. Cheng, and S. Fukusako (1991), Review of intrinsic thermophysical properties of snow, ice, sea ice and frost, in *Proceedings 3rd International Symposium on Cold Regions Heat Transfer*, edited by J. P. Zarling and S. L. Fausett, pp. 187–218, Univ. of Alaska, Fairbanks.

L. G. E. Backstrom, H. Eicken, and D. J. Pringle, Geophysical Institute, University of Alaska, P.O. Box 757320, Fairbanks, AK 99775-7320, USA. (larsg@gi.alaska.edu; hajo.eicken@gi.alaska.edu; pringle@gi.alaska.edu)

H. J. Trodahl, School of Chemical and Physical Sciences, Victoria University of Wellington, P.O. Box 600, Wellington, New Zealand. (joe.trodahl@vuw.ac.nz)